AIAA 94-2345

Turbulent Transonic Airfoil Flow Simulation Using An Improved Pressure Based Method With a $k-\varepsilon$ Turbulent Closure

G. Zhou, L. Davidson and E. Olsson
Thermo and Fluid Dynamics
Chalmers University of Technology
S-412 96 Gothenburg, Sweden

AIAA 25th
Fluid Dynamics Conference
June 20-23, 1994/Colorado Springs, CO

Turbulent Transonic Airfoil Flow Simulation Using An Improved Pressure Based Method With a $k-\epsilon$ Turbulent Closure

Gang Zhou, Lars Davidson and Erik Olsson
Thermo and Fluid Dynamics, Chalmers University of Technology,
S-412 96 Gothenburg, Sweden

The paper presents the performance of an improved pressure-based algorithm for turbulent transonic aerodynamic flow simulations. There are few successful computational reports for transonic airfoil flow worked out with the pressure-based method. In this study, an advanced approach based on a pressure correction scheme, which was validated earlier in solving the Euler equations, is extended to solve the Reynolds-averaged Navier-Stokes equations for turbulent transonic flow around the airfoil RAE 2822. An implicit numerical dissipation model is adopted to extract just enough dissipation mechanism from pressure gradients to damp the destabilizing numerical effects, without smearing the physical discontinuity at shocks. The standard $k-\epsilon$ turbulence closure with a near-wall one-equation model is used. The computational results are compared to experimental data. Several discretization schemes such as the second-order upwind, hybrid and MUSCL schemes for convection terms are investigated. The computational results show that the proposed pressure-based method has a comparable resolution for the turbulent transonic external aerodynamic flows to the time-marching methods.

1 Introduction

For a long time, most compressible aerodynamic flow simulations have been carried out with density-based methods (as time-marching methods are often called) in which density is used as a primary variable in the continuity equation, while pressure is extracted from the equation of the state. It is well known that this class of methods is inefficient for incompressible flow calculations, because the density variation in these regions becomes negligible, leading to convergence problems. On the other hand, pressure correction based methods[1–3] which use pressure as a dependent variable, show excellent performance in predicting of incompressible turbulent and chemically reacting flow.

For transonic flow simulations, however, some difficulties have been encountered due to the complicated nature of the flow, including both subsonic and supersonic regions as well as shocks. In recent years, many improvements have been made for pressure-based methods, such as non-staggered (collocated) grid arrangement,[2,5–7] the use of mass flux components $(\rho U, \rho V)$ as primary variables[8–10] instead of velocities (U, V) and advanced numerical artificial dissipation models.[4,5,8–10] Some successful results have been reported. However, most of them deal with internal flow simulation. A few[10–12] successful calculations for the transonic airfoil flow, which is the most challenging case for the demonstration of how well a pressure-based method can resolve physical discontinuities, such as external shocks, are available in the literature. In this work, an improved pressure correction based algorithm is demonstrated and validated for turbulent transonic airfoil flow computations using Reynolds averaged Navier-Stokes equations.

Among all the difficulties encountered when using the pressure-based method for predicting transonic flows, the most important issue is which type of and how much artificial dissipation should be included in the calculations in order to prevent the unphysical behavior which is caused by the elliptic nature of the pressure correction equation. How well a computational algorithm can capture the physical discontinuities depends on a proper choice of a numerical dissipation model. For the pressure-based method, one must find a mechanism for introducing just enough artificial dissipation to damp the unphysical behavior without smearing the physical discontinuity at shocks. Many efforts have been focused on this. For the density-based methods, it is well-known that a proper numerical dissipation model[13–15] should be a combination of fourth and second order differencing of the dependent variables. Some successful pressure-based methods[5,9,10] have also demonstrated (some directly and others indirectly) a similar requirement for the dissipation model.

This work uses an implicit artificial dissipation

model which consists of second and fourth order derivatives of pressure only, in all equations. The model was first adopted to test the airfoil flow calculations for the Euler equation in a previous paper.[10] It was found that two level filters should be used to adjust second-order dissipation for inviscid flow simulations. The results have shown a good capability of predicting both internal and external inviscid transonic flows. For the turbulent viscous flow case, only one level filter needs to be used, which introduces less amount of numerical dissipation. Consequently, the physical dissipation in this case dominates over the numerical dissipation, introduced by the second level filter used for the inviscid flow cases.

Many turbulence models have been designed, such as algebraic turbulence models,[17,18] a number of $k-\epsilon$ models[19] and Reynolds stress turbulence models, (often referred to as second moment closure). The major objective, here, is not to implement or evaluate a new turbulence model, but rather, use a standard $k-\epsilon$ turbulence closure with a one-equation model near the wall. The results of the prediction of the transonic flow around airfoil RAE 2822 for *case* 6, *case* 9 and *case* 10 of Cook et. al.[20] will be presented and discussed.

The main features of the proposed algorithm are:

* Using a collocated grid arrangement in which all variables are stored at the center of the cell. Since the convection contribution to the coefficients in the discretized equations is the same for all variables in this arrangement, it is attractive to employ high order differencing schemes.

* Solving for Cartesian mass flux components $(\rho U, \rho V)$. Since mass flux components $(\rho U, \rho V)$ vary smoothly across shocks, solving for mass flux components reduces discretization errors in the shock regions.

* Assuming constant stagnation enthalpy everywhere in the flow field. Since the maximum Mach number of the test cases is moderate ($\prec 1.4$), it is reasonable to assume that the viscous dissipation is relatively low.

* Adopting an implicit dissipation model, which mainly includes second and fourth order differencing terms expressed in pressure only.

* Standard two equation turbulence closure with a near-wall one equation model.

* Several schemes, such as hybrid, second-order upwind and MUSCL, for convective terms.

Following the description of the proposed scheme, the computational results, compared with the experimental data of airfoil RAE 2822, are presented.

2 Governing Equations and Turbulent Closure

The transonic mean flow is modeled by the Reynolds-averaged conservation equations of mass, momentum and energy. These mean equations, in terms of the Favre-averaged concept, can be expressed in Cartesian tensor form for ideal gas as[21]

$$\bar{\rho}_{,t} + \left(\bar{\rho}\tilde{u}_j\right)_{,j} = 0 \tag{1}$$

$$\left(\bar{\rho}\tilde{u}_i\right)_{,t} + \left[\bar{\rho}\tilde{u}_j\tilde{u}_i + \delta_{ij}\bar{P} - \left(\bar{\tau}_{ij} - \overline{\rho u_i^{"} u_j^{"}}\right)\right]_{,j} = 0 \tag{2}$$

$$\begin{aligned}\left(\bar{\rho}\tilde{H} - \bar{P}\right)_{,t} \quad &+ \quad \left[\tilde{u}_j\left(\bar{\rho}\tilde{H}\right) + \bar{q}_j + \overline{\rho u_j^{"} h^{"}}\right]_{,j} \\ &- \quad \left[\tilde{u}_i\left(\bar{\tau}_{ij} - \overline{\rho u_i^{"} u_j^{"}}\right)\right]_{,j} = 0\end{aligned} \tag{3}$$

where

$$\bar{\tau}_{ij} = \mu\left[\tilde{u}_{i,j} + \tilde{u}_{j,i} - \frac{2}{3}\delta_{ij}\tilde{u}_{m,m}\right] \tag{4}$$

$$\bar{\rho} = \frac{\gamma\bar{P}}{(\gamma-1)\left(\tilde{H} - 0.5\tilde{u}_i\tilde{u}_i\right)} \tag{5}$$

Here $\bar{\rho}$ is the mean density, $\bar{P}$ the mean pressure, $\tilde{u}_i$ the mean velocity in the direction of x_i, $\tilde{H}$ the total enthalpy per unit mass, and μ the coefficient of molecular viscosity. In the above equations, the overbar $(-)$ denotes Reynolds averaging and tilde $(\sim)$ denotes Favre averaging.

It will be assumed that the ratio of specific heats γ is constant, and that total enthalpy may be considered to be constant. Such an assumption is reasonable for the present moderate Mach number $(M \prec 1.4)$[22] cases. This assumption avoids solving the energy equation and modeling of turbulent heat fluxes. Therefore, the closure of the Reynolds-averaged equations only requires the modeling of Reynolds stresses (no need for modeling heat flux). Here the Boussinesq eddy viscosity assumption is used to express the Reynolds stresses tensor as :

$$\begin{aligned}\overline{\rho u_i^{"} u_j^{"}} \quad &= \quad -\mu_t\left[\tilde{u}_{i,j} + \tilde{u}_{j,i} - \frac{2}{3}\delta_{ij}\tilde{u}_{m,m}\right] \\ &+ \quad \frac{2}{3}\delta_{ij}\bar{\rho}\tilde{k}\end{aligned} \tag{6}$$

where μ_t is the eddy viscosity, and $\tilde{k}$ is the turbulent kinetic energy per unit mass:

$$\bar{\rho}\tilde{k} = \frac{1}{2}\overline{\rho u_i^{"} u_i^{"}}. \tag{7}$$

In the present study, the values of the eddy viscosity μ_t is estimated by solving two transport equations for the turbulent kinetic energy $\tilde{k}$ and its dissipation

rate ϵ :

$$\left(\bar{\rho}\tilde{k}\right)_{,t} + \left[\tilde{u}_j\left(\bar{\rho}\tilde{k}\right) - \left(\mu + \frac{\mu_t}{\sigma_k}\right)\tilde{k}_{,j}\right]_{,j} = P_k - (\bar{\rho}\epsilon) \quad (8)$$

$$(\bar{\rho}\epsilon)_{,t} + \left[\tilde{u}_j\left(\bar{\rho}\epsilon\right) - \left(\mu + \frac{\mu_t}{\sigma_\epsilon}\right)\epsilon_{,j}\right]_{,j} = \frac{\epsilon}{\tilde{k}}\left[c_{1\epsilon}P_k - c_{2\epsilon}\left(\bar{\rho}\epsilon\right)\right] \quad (9)$$

where the production term has the form:

$$P_k = -\overline{\rho u_i'' u_j''}\tilde{u}_{i,j} \quad (10)$$

and the eddy viscosity, away from the wall, is modeled as

$$\mu_t = c_\mu \bar{\rho}\frac{\tilde{k}^2}{\epsilon}. \quad (11)$$

The standard $k-\epsilon$ model is unable to model low Reynolds number turbulent flow near the wall. Many near wall treatments[19] can be chosen to calculate k and ϵ down to the wall. A near-wall one-equation model for the turbulent kinetic energy, which was suggested by Wolfshtein[23] and modified by Chen and Patel[24] has been tested by many researchers, Refs. 21, 25–27. Such an one-equation near-wall model is applied in this study. The model defines two different length scales l_μ and l_ϵ, one for turbulent stress and one for turbulent dissipation. Then, the dissipation rates of the turbulent kinetic energy and the eddy viscosity are modeled by

$$\epsilon = \frac{\tilde{k}^{3/2}}{l_\epsilon} \quad (12)$$

and

$$\mu_t = \bar{\rho}c_\mu \tilde{k}^{1/2} l_\mu. \quad (13)$$

Therefore, close to the wall, the closure of the Reynolds averaged equations with the one-equation model is reduced to solving the k-equation and specifying the turbulent dissipation length scale l_ϵ and turbulent length scale l_μ.

An exponential expression,[23,24] is used to combine the viscous sublayer and inner-layer dissipation length scale, and turbulent length scales as:

$$l_\mu = C_l y_n\left[1 - exp\left(\frac{-\tilde{k}^{1/2}y_n}{2C_l\,\nu}\right)\right] \quad (14)$$

$$l_\epsilon = C_l y_n\left[1 - exp\left(\frac{-\tilde{k}^{1/2}y_n}{A_\mu\,\nu}\right)\right] \quad (15)$$

$$C_l = \kappa C_\mu^{-3/4} \qquad A_\mu = 70 \quad (16)$$

where y_n is the normal distance from the wall. The matching position between the viscous sublayer and the outer region is chosen along a fit grid line where the minimum value of the term $\tilde{k}^{1/2}y_n/\nu$ is of order 250.

In the present turbulent closure modeling the constants are :

$$c_\mu = 0.09; \quad c_{1\epsilon} = 1.44; \quad c_{2\epsilon} = 1.92; \quad \sigma_k = 1.0; \quad \sigma_\epsilon = 1.3. \quad (17)$$

3 Numerical Approach

The governing equations given above can be cast into the standard transport equation for a general dependent variable Φ (here, the bars indicating the averaging are dropped), in Cartesian coordinates as

$$\Phi_{,t} + (U_i\Phi)_{,i} = \left[\Gamma_\Phi\left(\frac{\Phi}{\rho}\right)_{,i}\right]_{,i} + S^\Phi \quad (18)$$

where Φ can be the Cartesian mass flux components, turbulent kinetic energy, dissipation rate of turbulent kinetic energy, *etc.*, Γ_Φ is the effective diffusivity, and S_Φ denotes the source per unit volume for the dependent variables Φ.

3.1 Discretization

Integrating Eq.(18) over a control volume, by using the Gaussian theorem, we get the following discretized equation

$$\left(\Phi - \Phi^0\right)\frac{\delta v}{\triangle t} + \sum_m\left(\mathbf{F}\bullet\mathbf{A}\right) - \sum_m\left(\Gamma_\Phi\nabla\Phi\bullet\mathbf{A}\right) = S_\Phi\delta v \quad (19)$$

where $\mathbf{F} = (\rho\mathbf{V}, \mathbf{V}\Phi)^T$ is the flux tensor, δv the volume of the cell, and Φ^0 the value at previous time level, and m refers to each face $\mathbf{A}$ of the control volume. The discretizing equation can be cast into standard form (See 6, 10)

$$a_P\Phi_P = \sum a_{nb}\Phi_{nb} + S_C^\Phi \quad (20)$$

where subscript nb denotes neighbor and

$$a_P = \sum a_{nb} - S_P^\Phi.$$

The coefficients a_{nb} contain contributions from both convection and diffusion. S_C^Φ and S_P^Φ contain the remaining terms. When Eq. (19) is cast into Eq.(20), some additional source terms S_C^Φ and S_P^Φ must be considered, due to the choice of dependent variables as mass flux components, and due to the choice of full description of the stress tensor.

The first addition term is referred to as the *convecting source term* which represents the errors of the convection parts of coefficients a_{nb} over the control volume.[1] Since the convection does not include density in this variable option, it is also referred to as "*volume errors*" instead of *mass errors*. It can be written

$$\left(S_P^\Phi\right)_{add1} = \sum_m\left[\frac{(\rho\mathbf{V})\cdot\mathbf{A}}{\tilde{\rho}}\right]_m$$

This term has to be added onto S_P^Φ. It should be pointed out that in order to balance the discretized equation, the retarded density[28] $\tilde{\rho}$ should be used in the term $\left(S_P^\Phi\right)_{add1}$, since the left hand of Eq. (20) has adopted the numerical model which includes the retarded density.

The second additional term is referred to as the *diffusion source term*, due to the adoption of a full description of the stress tensor Eqs (4) and (6). This term

$$\begin{aligned}\left(S_C^\Phi\right)_{add2} &= \left[(\mu+\mu_t)\left(\tilde{u}_{j,i}-\frac{2}{3}\delta_{ij}\tilde{u}_{m,m}\right)\right]_{,j} \\ &- \frac{2}{3}\delta_{ij}\left(\bar{\rho}\tilde{k}\right)_{,j}\end{aligned}$$

is added to S_C^Φ. At boundaries, the values of the derivative of the terms in brackets [ ] and ( ) have been obtained by extrapolating from the inner field.

The third additional term is referred to as the *compressible source term* due to a decoupling of the derivative of mass flux and velocity. It is shown explicitly as follows

$$\Gamma_\Phi \frac{\partial}{\partial x_j}\left(\frac{\Phi}{\rho}\right) = \frac{\Gamma_\Phi}{\rho}\frac{\partial \Phi}{\partial x_j} + \frac{\Gamma_\Phi \Phi}{\rho^2}\frac{\partial \rho}{\partial x_j}.$$

The third source term consists of the second terms on the right hand side in the above equation. For smooth density variations, the term is negligible. Therefore, this term is important only in varying gradient regions, such as shocks.

It should be noticed that the first term is crucial to momentum conservation and numerical stability. At shocks, the third source term is also important.

3.2 Numerical Dissipation

There are a variety of numerical dissipation models which are used to suppress spurious odd and even point oscillations and to damp unphysical overshoots near shock waves. Most of them use a combination of second and fourth order terms of the dependent variables Φ, $(\rho, \rho U, \rho V$ and $\rho E)$, either explicitly or implicitly. In this study, an implicit numerical dissipation model is used which just includes the second and fourth order terms expressed in pressure for all transport equations. The fourth-order terms of the numerical dissipation model are due to the use of Rhie-Chow interpolation,[2] and the second-order terms are due to the use of retarded density,[9,28] which is equivalent to the retarded pressure concept.[8] It can been shown that the model, for uniform grid and two-dimensional flow, can be written explicitly[10]

$$DP = D_x P + D_y P \tag{21}$$

where $D_x P$ and $D_y P$ are the contributions for the two coordinate directions, respectively, which have the form (for $U_\eta, U_\xi > 0$):

$$D_x P = \left\{d_{i+1/2,j} - d_{i-1/2,j}\right\};$$

$$D_y P = \left\{d_{i,j+1/2} - d_{i,j-1/2}\right\} \tag{22}$$

The $d's$ in the above equation can be written

$$\begin{aligned}d_{i+1/2,j} &= A_x \mu_{i+1/2}\left(P_{i+1/2,j} - P_{i-1/2,j}\right) \\ &+ B_x\left(P_{i+2,j} - 3P_{i+1,j} + 3P_{i,j} - P_{i-1,j}\right)\end{aligned} \tag{23}$$

where A and B are coefficients imposed by momentum and state equations, and $\mu_{i+1/2}$ is a smoothing function due to the use of retarded density[28] which reads

$$\tilde{\rho} = \rho - \mu \Delta x \vec{\rho}_x. \tag{24}$$

A two-level filtering smoothing function has been designed[10] as

$$\begin{aligned}\mu_{i+1/2} = \max\Bigg\{0.0,\, K_1\left[1-\left(\frac{M_{ref}}{M_{i+1/2,j}}\right)^2\right] \\ + K_2\left[1-\left(\frac{\Upsilon_{ref}}{\Upsilon_{i+1/2,j}}\right)^2\right]\Bigg\}\end{aligned} \tag{25}$$

where

$$\Upsilon_{i+1/2,j} = \max\left(\Upsilon_{i+1,j}, \Upsilon_{i,j}\right)$$

and

$$\Upsilon_{i,j} = \frac{\left|P_{i+1,j} - 2P_{i,j} + P_{i-1,j}\right|}{\left|P_{i+1,j} + 2P_{i,j} + P_{i-1,j}\right|}$$

It was found that only one level filter is needed for turbulent flow calculations to switch on the second-order dissipation which is needed to enhance the stability in supersonic regions. The constant dominating second-level filter was set at zero.

The numbers $K_1 = 1.$, $K_2 = 0.$ and $M_{ref} = 1.0 \sim 1.10$. The details of the present model are given in the Appendix in Refs.10, 12.

3.3 Pressure Correction Equation

In this study, mass flux components instead of velocities, are selected as the dependent variables. Such a variable option allows for a direct relationship between momentum and pressure by truncating the momentum equations in the same way as in the conventional SIMPLE method[1,6]

$$\mathbf{A}\cdot(\rho\mathbf{V})' = -\frac{\delta v}{a_P}\mathbf{A}\cdot\nabla P'. \tag{26}$$

where $'$ means correction terms.

In order to enhance stability of the original pressure correction equation, the density correction is taken as[8]

$$\rho' = \frac{\gamma P'}{(\gamma-1)\left(H_0 - 0.5|\mathbf{V}|^2\right)}. \tag{27}$$

Therefore, the pressure correction equation becomes

$$\rho'_P \frac{\delta v}{\triangle t} + \sum_{m=1}^{4}\left(\frac{\delta v}{a_P}\mathbf{A}\cdot\nabla P'\right) + \triangle \dot{m}_P = 0 \tag{28}$$

where $\triangle \dot{m}_P$ is the continuity error.

This manipulation gives the pressure correction equation a hyperbolic appearance with respect to time. As Mach number becomes small and density gradients become negligible, the quasi-time-dependent term disappears and the scheme degenerates to the standard iterative scheme for incompressible flow.

In the curvilinear coordinates, the diffusion term of Eq. (28) forms

$$(\mathbf{A} \cdot \nabla P')_{i+1/2} = \left\{ \mid \mathbf{A} \mid \mathbf{n} \cdot \mathbf{g}_1 g^{1j} \frac{\partial P'}{\partial \xi_j} \right\}_{i+1/2}$$

which can be rewritten so that

$$\{\mathbf{A} \cdot \nabla P'\}_{i+1/2} = D_{\xi i+1/2} \left(P'_{i+1} - P'_i\right) + D_{\eta i+1/2} \left(P'_{i+1/2,j+1/2} - P'_{i+1/2,j-1/2}\right)$$

where the D's contain the metrics of the grid. The discretized equation for P' can also be cast into the form

$$a_P P'_P = \sum a_{nb} P'_{nb} + S_C \qquad (29)$$

where S_C is mass residual.

Since the pressure correction equation has been already discussed in many references, other aspects of the discretization of this equation are omitted here. The detailed discretization of Eq. (28) is performed in a way similar to the diffusion terms of Eq. (18) (See 6, 10).

3.4 Initial and Boundary Conditions

The calculations start from a uniform free stream condition for all variables.

Boundary conditions everywhere, except at solid walls, are applied by using the same strategy as in solving the Euler equations.[10] At the far field, the locally one-dimensional Riemann invariants, entropy and tangential velocity component are obtained by using the theory of characteristics. A far field circulation correction based on the compressible potential vortex solution is used to modify free stream velocity. On solid walls, no-slip and zero turbulent energy boundary conditions are applied. A first-order extrapolation is adopted for both pressure and pressure correction at the wall. The values of k, ϵ and pressure correction at the outlets are extrapolated from the inner field.

4 Results and Discussion

Three calculation cases are examined for airfoil RAE 2822, which has been extensively investigated experimentally by Cook *et al.* and computationally by many aerodynamists. All cases use a 256×64 C-grid with 208 cells on the airfoil's surface and finer clustering near the leading and trailing edges. The grid extent is about 10 chords in all directions. The normal spacing of the first point off the wall is of the order 1×10^{-5} of the chord which corresponds to $O(y^+)$. For

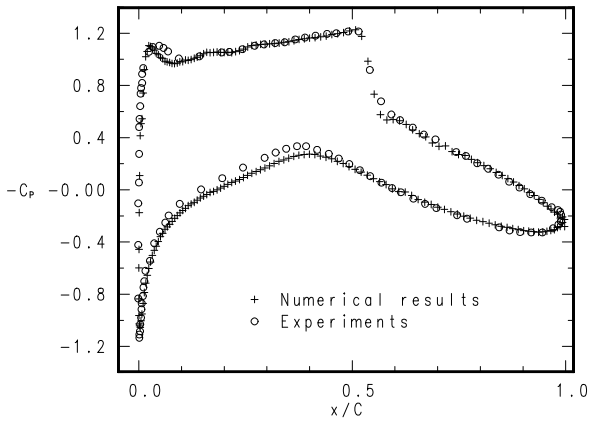

Figure 1. Pressure distributions for RAE 2822 case 6, MUSCL scheme

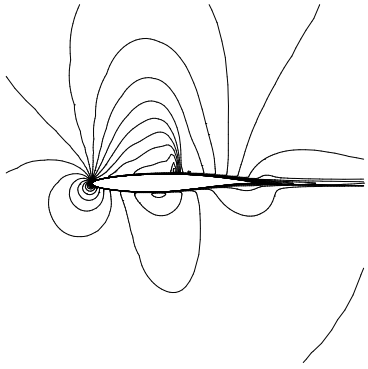

Figure 2. Mach number contours case 6, MUSCL scheme

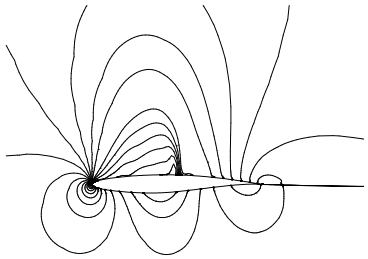

Figure 3. Pressure contours, case 6, MUSCL scheme

all cases the pure MUSCL[33] scheme, namely for the convective terms of both momentum and $k-\epsilon$ equations, is adopted first. Then, the calculations using the pure hybrid scheme[1] and second-order upwind schemes LUDS[34,35] or the combination of hybrid and second-order upwind are also performed and will be discussed later.

In the first case referred to as *case* 6 of Ref. 20 is $M = 0.725, R_e = 6.5 \times 10^6$ and the flow at a angle of attack $\alpha = 2.92$ deg (uncorrected). The transition location for this case is fixed at $x/C = 0.03$, the same as in the experimental data. Since the calculations are carried out in free flow, the angle of attack must be corrected from the geometrical angle of attack due to the presence of wind tunnel interference. Various types of correction on Mach number and angle of attack have been proposed in airfoil flow simulation.[31] In this calculation, the corrected angle of attack is chosen as $\alpha = 2.60$ which is the same as in Ref. 11, while no correction is made for the free stream Mach number. Figure 1 shows the pressure coefficient distributions on the upper and lower airfoil surfaces from the present calculations in comparison with experiment data. The Mach number contours are shown in Figure 2, and the pressure contours are shown in Figure 3.

It can be seen that the computed results show good agreement with the experiments. A sharp discontinuity in appearance is achieved successfully for both shock strength and location. On the lower surface of the airfoil the pressure is slightly overpredicted. such a feature is common in almost all the computational results in Ref. 31. The results shown in Ref. 11 which also used the pressure-based method have shown better agreement with experiments on the lower surface of this airfoil, but the shock strength and location was underpredicted.

A another difficulty in this computation with the exception of shock location, is a proper prediction of pressure distribution in the transition region on the upper surface of the airfoil. The presented results show that the peak at the transition point and at the wavy pattern of pressure on the upper surface agree very well with experiments. Just after the transition point, pressure is slightly overpredicted.

The second case presented corresponds to *case* 9 of Ref. 20, in which $M = 0.73$, $R_e = 6.5 \times 10^6$, and $\alpha = 3.19$ deg (uncorrected). The transition location is at $x/C = 0.03$. The corrected angle of attack is chosen as $\alpha = 2.80$. The Computed pressure coefficient, Mach number and pressure contours are compared with the experiment in Figure 4-6. Again, a good agreement with experiments is achieved for both shock strength and location. Down stream the transition point, the wavy pattern of pressure shows a tendency similar to that in experimental data. It can be seen that the discrepancy between numerical results and experiments just after the transition point increases.

The last case referred to as *case* 10 of Ref.20 is

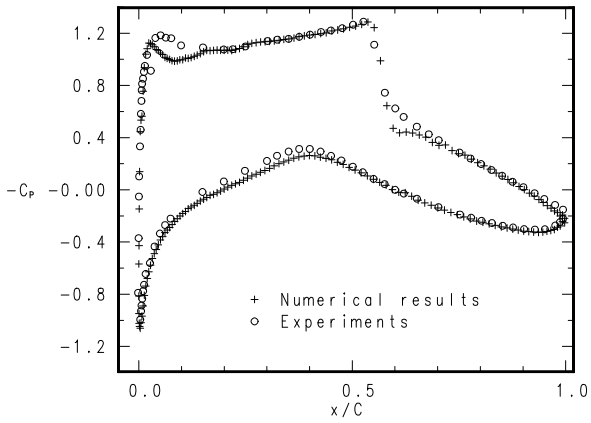

Figure 4. Pressure distributions for RAE 2822 case 9, MUSCL scheme

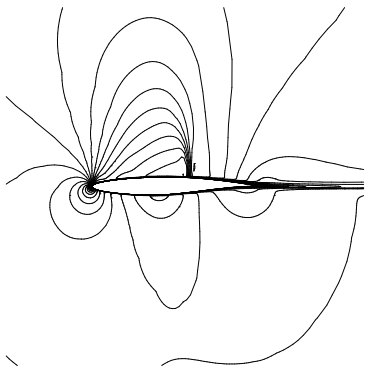

Figure 5. Mach number contours case 9, MUSCL scheme

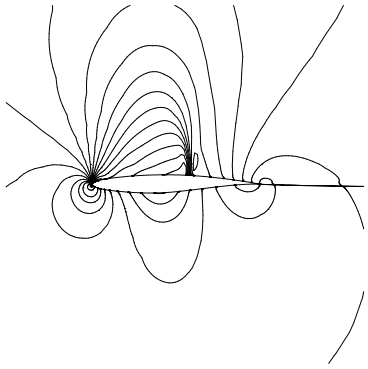

Figure 6. Pressure contours, case 9, MUSCL scheme

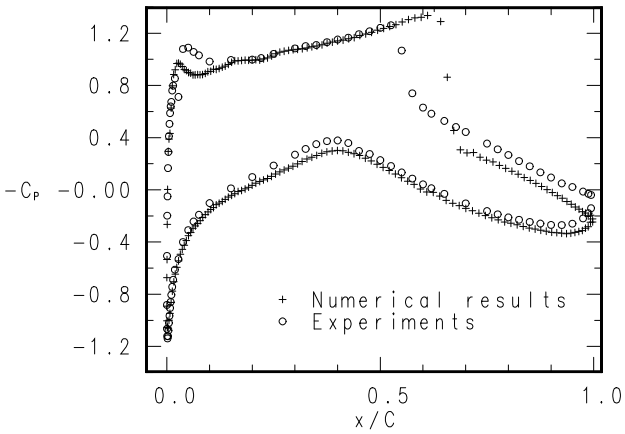

Figure 7. Pressure distributions for RAE 2822 case 10, MUSCL scheme

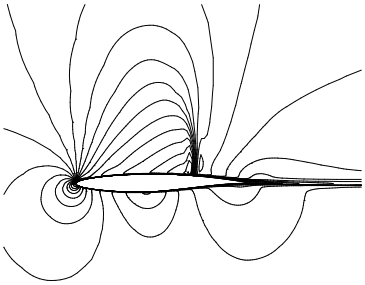

Figure 8. Mach number contours case 10, MUSCL scheme

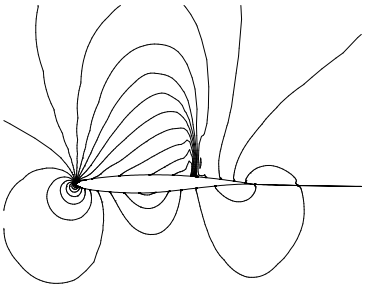

Figure 9. Pressure contours, case 10, MUSCL scheme

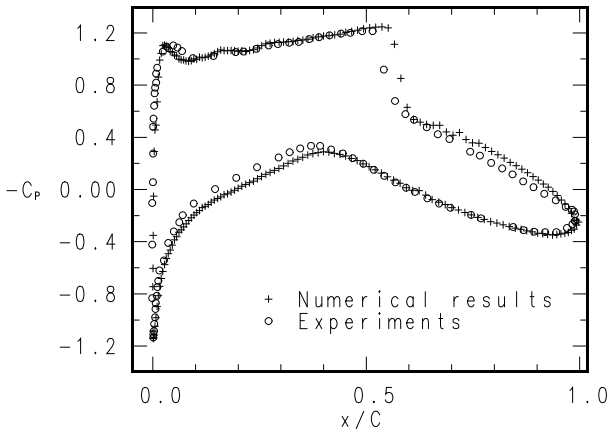

Figure 10. Pressure distributions for RAE 2822 case 6, hybrid scheme

$M = 0.75, R_e = 6.2 \times 10^6$, and $\alpha = 3.19$. This is the most difficult RAE 2822 case, since the shock wave causes a significant amount of boundary-layer separation. In this calculation, the corrected angle of attack is chosen as $\alpha = 2.57$. Figure 7 compares computed pressure coefficient distributions with experimental data. Almost all the calculations have overpredicted the shock strength and the location.[31,21,27] The presented results also show the same tendency. After the shock on the upper surface of the airfoil the pressure is overpredicted similarly to the results obtained from any of the density-based methods. This indicates that the numerical error involved in the pressure-based method is of comparable order to that in the time-marching method for this case.

On the other hand, the fact that both pressure-based and density-based methods overpredict the shock strength and its location indicates that the discrepancy between numerical results and experiments in the case with the strong shock, must be due to modeling errors, most probably in the turbulence model, or experimental uncertainties. The Mach number and pressure contours are shown in Figures 8 and 9. The transition location for this calculation is still at $x/C = 0.03$. It can be seen that the pressure in the transition region is overpredicted. Such an overprediction shows a tendency similar to the results of Refs. 21 and 27, which also used an one-equation turbulence model near the wall.

In order to investigate the difference in performance between different schemes, hybrid[1] and second-order linear upwind schemes (LUDS)[34,35] are also used for calculating all the cases. Results show that there are no significant differences between these schemes in the global results and the pattern of iso-lines of Mach number and pressure for the moderate shock *case* 6 and *case* 9. For *case* 10 some differences in the shock location and the pressure peak at the transition region appear as will be discussed below.

It should be mentioned that some adjustment

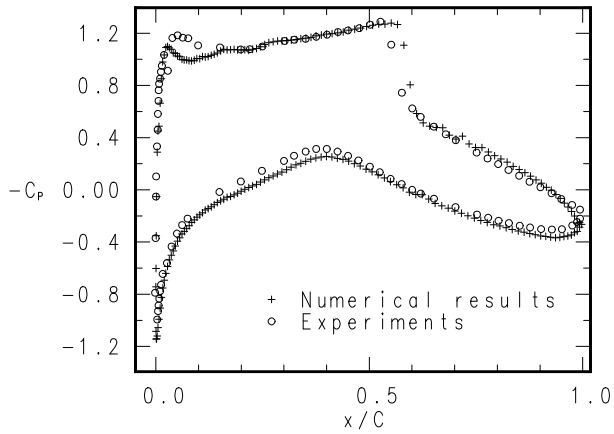

Figure 11. Pressure distributions for RAE 2822 case 9, hybrid scheme

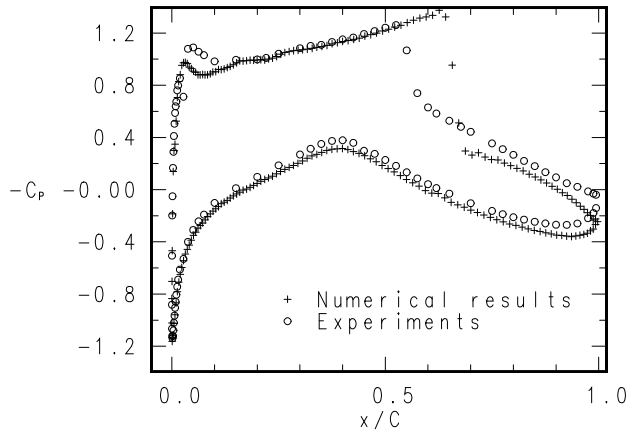

Figure 12. Pressure distributions for RAE 2822 case 10, hybrid scheme

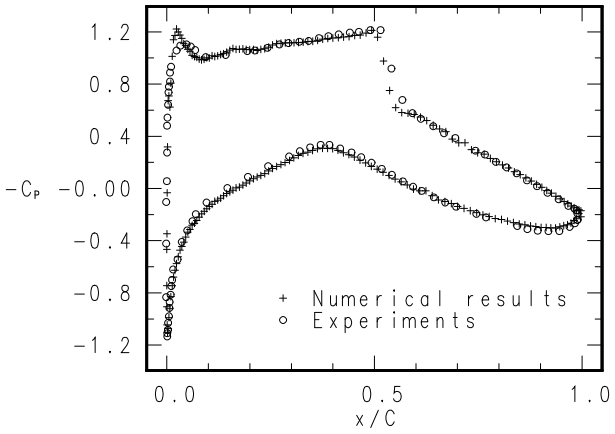

Figure 13. Pressure distributions for RAE 2822 case 6, LUDS scheme

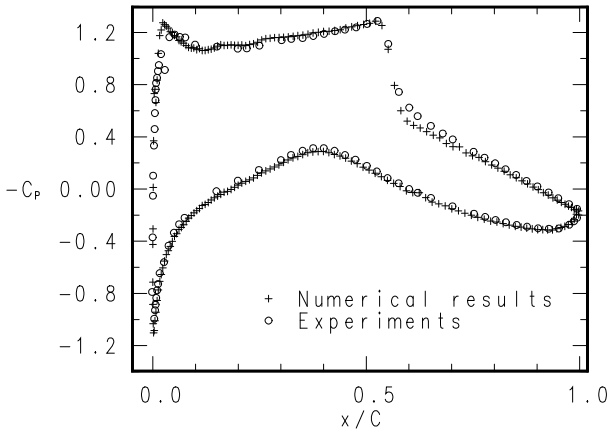

Figure 14. Pressure distributions for RAE 2822 case 9, LUDS scheme

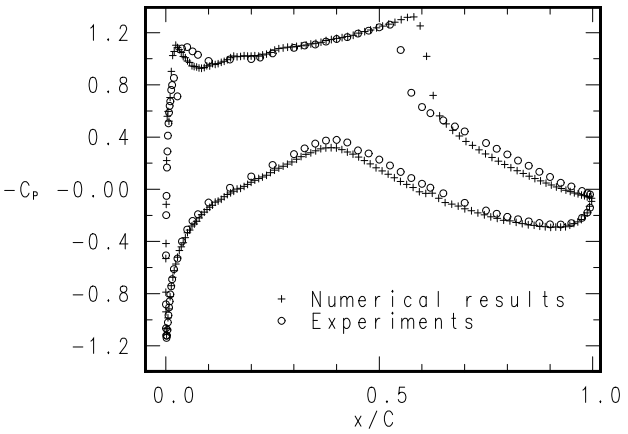

Figure 15. Pressure distributions for RAE 2822 case 10, LUDS scheme

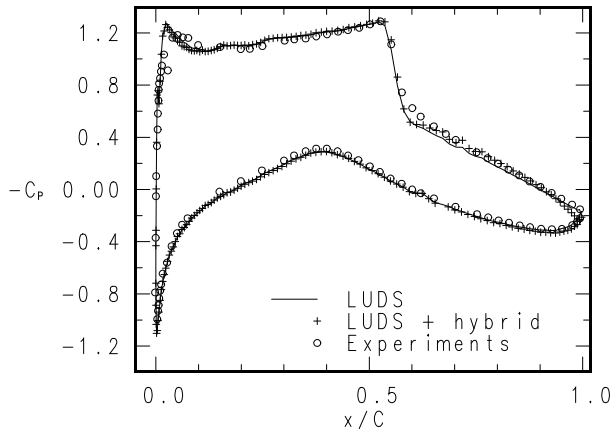

Figure 16. Pressure distributions for case 9 Comparison between LUDS and LUDS/hybrid schemes

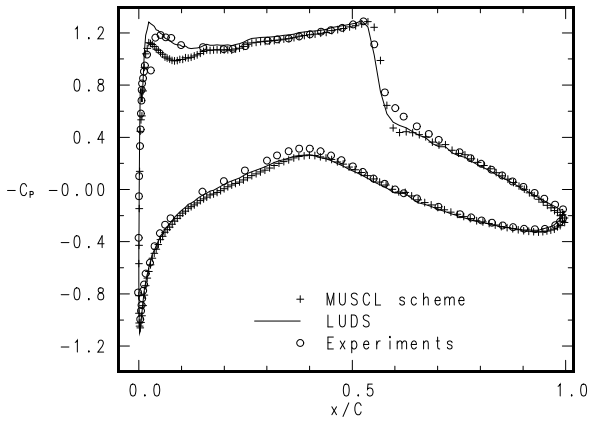

Figure 17. Pressure distributions for case 9 Comparison between MUSCL and LUDS schemes With same constant, $M_{ref} = 1.04$

of the constant M_{ref} in the smoothing function are needed. In the MUSCL scheme, $K_1 = 1.$, $M_{ref} = 1.04$ for *case* 9. In the hybrid scheme $K_1 = 1.$, $M_{ref} = 1.06$. And in the upwind scheme $K_1 = 1.$, $M_{ref} = 1.05$. Such a adjustment indicates that slightly more dissipation is needed in the MUSCL scheme. an adjustment of constants like this can be accepted as each scheme includes different amounts of numerical dissipation. Therefore, the amount of dissipation needed to be added to the calculations depends on which scheme will be used. The pressure coefficient distribution obtained from the pure hybrid scheme is presented in Figures 10 to 12. Figures 13 to 15 show the predicted pressure coefficient distribution from the second-order upwind scheme.

Comparing Figures 1, 4, 7 and Figures 10, 11, and 12, we can see that a similar resolution of negative pressure peak at the transition region has been achieved with both the hybrid and MUSCL schemes. The hybrid scheme is significantly better at predicting the pressure distribution on the lower surface of the airfoil. But the shock location and the pressure after the shock on the upper surface of the airfoil are underpredicted a little, as is shown in the figures.

The unbonded second-order upwind scheme[34,35] shows an impressive ability to predict pressure distribution on almost the entire surface of the airfoil in all cases, except for a slightly retarded prediction of the shock location in *case* 10. No numerical stability problems occur. The most interesting performance of the second-order upwind scheme is that the scheme can capture the negative pressure peak at the transition point in a much better way than the other two schemes. As shown in the figures, the negative pressure peak pierces through experiment data. Considering that the predicted pressure distribution just after the transition point follows data with a satisfactory accuracy, this indicates that a sharper peak might be more acceptable since there is a sharp stimulus at the transition point.

Figure 16 shows the comparison between the results obtained from pure second-order upwind scheme and those from the combination of hybrid scheme for the $k-\epsilon$ equations and second-order upwind scheme for momentum equations. From this figure we can see that there is no significant difference between these two computations. The reson for this is fact that $k-\epsilon$ equations are dominated by diffusion and source terms. Therefore, the choice of a discretization scheme for relatively small convection terms does not influence the global calculated flow field much. Nevertheless, the resolution of the pressure just after the transition point is lower in the latter computation.

It is noticed that the computational results are not very sensitive to the numerical constant M_{ref}. Figure 17 shows the results from the second-order upwind scheme with $M_{ref} = 1.04$ compared with Figure 14 with $M_{ref} = 1.05$. A comparison of MUSCL and LUDS schemes with the same constant, M_{ref}, is also shown in this figure. The main difference is in the resolution of the pressure at the transition region. It seems that the limiter in the MUSCL scheme, constructed so to make the scheme bounded in order to avoid non-physical oscillations, implicitly introduce too much numerical dissipation in this region where the pressure has a reverse gradient.

5 Concluding Remarks

A pressure-based method using a $k-\epsilon$ turbulence closure with a one-equation model near the wall has been used to calculate the turbulent transonic flow over an airfoil. An implicit nonlinear dissipation model was successfully used in different schemes to suppress oscillation without smearing the physical discontinuity at shocks. To substantiate the validity of the proposed method, three calculations for the airfoil RAE 2822 have been carried out. The computational results obtained from the proposed method, with several second-order discretized schemes, have shown a good agree-

ment with experimental data compared with density-based methods. Among the schemes adapted, the second-order upwind scheme has shown the sharpest behavior. The pressure on the lower surface obtained from the MUSCL and the hybrid scheme was slightly overpredicted.

One important conclusion that can be drawn from this work is that an advanced pressure-based method is also capable of predicting turbulent transonic aerodynamic flows around airfoils, even though its popularity is due mainly to its excellent performance in predicting incompressible turbulent flows. Some improvement including convergence acceleration and advanced turbulence modeling should be undertaken for the proposed method in the future.

References

[1] Patankar, S. V., "*Numerical Heat Transfer and Fluid Flow*", McGraw-Hill, Washington, 1980.

[2] Rhie, C. M., "A Pressure Based Navier-Stokes Solver Using the Multigrid Method", AIAA paper 86-0207, January, 1986.

[3] Shyy, W. and Chen, M. H., "Pressure-Based Multigrid Algorithm for Flow at All Speeds", *AIAA Journal*, Vol. 30, 1992, pp. 2660-2669.

[4] Rhie, C. M. and Chow, W. L., "Numerical Study of the Turbulent Flow Past an Airfoil with Trailing Edge Separation", *AIAA Journal*, Vol. 21, 1984, pp. 1527-1532.

[5] Chen, Y. S., "Viscous Flow Computations Using A Second-Order Upwind Differencing Scheme", AIAA paper, 88-0417, January, 1988.

[6] Davidson, L. and Farhanieh, B., "A Finite-Volume Code Employing Collocated Variable Arrangement and Cartesian Velocity Components for Computation of Fluid Flow and Heat Transfer in Complex Three-Dimensional Geometries", Rept. 92/4, Thermo and Fluid Dynamics, Chalmers University of Technology, Gothenburg, 1992.

[7] Perić, M., "A Finite Volume Method for the Prediction of Three-dimensional Fluid Flow in Complex Ducts", PhD Thesis, University of London, 1985.

[8] Mcguirk, J. J. and Page, G. J., "Shock Capturing Using a Pressure-Correction Method", *AIAA Journal*, Vol. 28, 1990, pp. 1751-1757.

[9] Lien, F. S. and Leschziner, M. A., " A Pressure-Velocity Solution Strategy for Compressible Flow and Application to Shock/Moment Turbulence Closure", *Journal of Fluid Engineering* , Vol. 115, 1993, pp. 717-725.

[10] Zhou, G. and Davidson, L., "A Pressure Correction Based Euler Scheme for Internal and External Transonic Flow Simulation", Submitted to *Journal of Computational Fluid Dynamics*, 1994.

[11] Lai, Y. G., So, R.M.C. and Przekwas, A. J., "Aerodynamic Flow Simulation Using a Pressure-Based Method and a Two-Equation Turbulence Model", AIAA paper 93-2902, July, 1993.

[12] Zhou, G., "Numerical Simulation for Transonic Flows with Special Emphasis on Development of Pressure-Based Method to Aerodynamic Flow", Lic. thesis for Engi., Rept. 93/94, Thermo and Fluid Dynamics, Chalmers University of Technology, Gothenburg, 1993.

[13] Jameson, A., Schmidt, W. and Turkel, E., "Numerical Solutions of the Euler Equations by Finite Volume Methods Using Runge-Kutta Time-Stepping Schemes," AIAA paper 81-1259, June, 1981.

[14] Rizzi, A., "Spurious Entropy and Very Accurate Solutions to the Euler Equations", AIAA Paper 84-1644, Janary, 1984.

[15] Pulliam, T. H. and Barton, J. T., "Euler Computations of AGARD Working Group 07 Airfoil Test Cases", AIAA paper 85-0018, January, 1985.

[16] Zhang, H. S. and So, R. M. C., Speziale, C. G. and Lai, Y. G., "Near-Wall Two-Equation Model for Compressible Turbulent Flows", *AIAA Journal*, Vol, 31, 1993, pp. 196-199.

[17] Cebeci, T. and Smith, A. M. O., *Analysis for Turbulent Boundary Layers*, Academic Press, NewYork, 1974.

[18] Baldwin, B. and Lomax, H., "Thin-Layer Approximation and Algebraic Model for Separated Turbulent Flows", AIAA paper 78-257, January, 1978.

[19] Patel, V. C., Rodi, W. and Scheuerer, G., "Turbulent Models for Near-Wall and Low Reynolds Number Flows: A Review", *AIAA Journal*, Vol, 23, 1985, pp. 1308 -1318.

[20] Cook, P. H., McDonald, M. A., and Firmin, M. C. P., "Aerofoil RAE 2822–Pressure Distributions, and Boundary Layer and Wake Measurements," AGARD Advisory Report No.138., 1979.

[21] Mitcheltree, R. A., Salas, M. D. and Hassan, H. A., "One-Equation Turbulence Model for Transonic Airfoil Flows", *AIAA Journal*, Vol, 28, 1990, pp. 1625-1632.

[22] Lien, F. S., "Computational Modeling of 3D Flow in Complex Ducts and Passages", Thesis for PhD, February, 1992.

[23] Wolfshtein, M., "The Velocity and Temperature Distribution in One-Dimensional Flow with Turbulence Augmentation and Pressure Gradient", *Int. J. Mass Heat Transfer*, Vol. 12, 1969, pp. 301-318.

[24] Chen, H. C. and Patel, V. C., "Practical Near-wall Turbulence Models for Complex Flow Including Separation", AIAA paper 87-1300, Honolulu, June, 1987.

[25] Davidson, L. and Rizzi, A., "Navier-Stokes Computation of Airfoil in Stall Using Algebraic Reynolds- Stress Model", *J. Space and Rochets*, Vol. 79, 1992, pp. 794-800.

[26] Davidson, L., "Reynolds Stress Transport Modeling of Shock/Boundary-Layer Interaction", AIAA paper 93-2936, July, 1993.

[27] Hellström, TH., Davidson, L. and Rizzi, A., "Reynolds Stress Transport Modeling of Transonic Flow Around the RAE2822 Airfoil", AIAA-paper 94-0309, 32th Aerospace Sciences Meeting, Reno, Jan 1994.

[28] Wornom, S. F. and Hafez, M., "Calculation of Quasi-one-dimensional Flows With Shocks", *Computers and Fluids*, Vol. 14, No. 2, 1986. pp. 131-140.

[29] Simpson, R., "Two-Dimensional Turbulent Separated Flow", AGARDograph No.287 Vol.1, 1985.

[30] Launder, B. E. and Spalding, D. B., "The Numerical Computation of Turbulent Flows", *Computer Methods in Applied Mechanics and Engineering*, Vol. 3, 1975, pp. 269-289.

[31] Holst, Terry L., "Viscous Transonic Airfoil Workshop Compendium of Results", *AIAA Journal*, Vol, 25, 1988, pp. 1073-1087.

[32] Johnson, D. A. and King, L. S., "A Mathematically Simple Turbulence Closure Model for Attached and Separated Turbulent Boundary Layers", *AIAA Journal*, Vol, 23, 1985, pp. 1684-1692.

[33] van Leer, B., "Towards the Ultimate Conservation Difference Scheme V, A Second-order Sequel to Godunov's Method", *Journal of Computational Physics*, Vol. 32, 1979, pp. 101.

[34] Shyy, W., Thakur, S. and Wright, J. "Second-order Upwind and Central Difference Schemes for Recirculating Flow Computation", *AIAA Journal*, Vol, 30, 1992, pp. 923-932.

[35] Lien, F-S and Leschziner, M. A., "Approximation of Turbulence Convection in Complex Flows with A TVD-MUSCL Scheme", Proc. 5th Int. IAHR Symp. on Refined Flow Modeling and Turbulence Measurements, pp. 183-190, Paris, Sept. 1993.

[36] Issa, R. I., "Solution of the Implicitly Discretized Fluid Flow Equations by Operator-Splitting", *Journal of Computational Physics,* Vol. 62, 1986, pp. 40-65.

[37] Leonard, B. P., "A Stable and Accurate Convective Modeling Procedure Based on Quadratic Upstream Interpolation", *Computer Methods in Applied Mechanics and Engineering*, Vol. 19, 1979, pp. 59-97.